Solid State Electronics 151 (2019) 11–17

Contents lists available at ScienceDirect

Solid State Electronics

journal homepage: www.elsevier.com/locate/sse

Process optimization and device variation of Mg-doped ZnO FBARs

Franklin Li Duan[a,*], Zhi Yang[a], Zhonglin Ji[a], Haotian Weng[a], Ziyi Xie[a], Allegro Shen[a], Shijie Mi[a], Xi Chen[a], Yigang Chen[b], Qianhui Liu[b]

[a] School of Electronic Information and Electrical Engineering, Shanghai Jiao Tong University, Shanghai 200240, China
[b] School of Materials Science and Engineering, Shanghai University, Shanghai 200444, China

ARTICLE INFO

Keywords:
Piezoelectric
FBAR
RF resonator
Bulk wave effects & devices

ABSTRACT

Thin film bulk acoustic resonator (FBAR) plays a very important role in radio frequency (RF) filters used in cell phone and other wireless systems. Although FBAR is commercialized, the design/process interactions on the frequency response variation in FBAR device are still lacking. Design and fabrication are two crucial aspects affecting FBAR device performance. In this report, various solidly mounted resonators (SMR) were designed, fabricated and analyzed to study wafer-level site-to-site RF variation on design and fabrication process. As a key process step for SMR FBAR, the optimization process of Mg-doped ZnO piezoelectric thin film deposition was studied by varying thin film sputtering conditions using various sputtering targets and by post annealing treatment after the deposition. The quality of this crucial layer was verified by XRD on its (0 0 2) crystallization and wafer-level FBAR RF characterization. FBAR devices with high quality were fabricated with an excellent resonant behavior near 2 GHz and a maximum return loss of −15 to 25 dB. Quality factor Q ranges from 400 to 800, with a coupling coefficient $keff^2$ of 1.5–3%. Wafer-level and wafer-to-wafer variation of central frequency are within 1.8–2.1 GHz. Computer simulation verified that this frequency variation correlates to the piezoelectric film variation of 1.6–1.9 μm. Process control on this piezoelectric thin film is essential to maintaining the resonator frequency-controlled value when building duplexer RF circuits. The dependency of RF performance on FBAR size, density and orientation is not obvious, compared to that of the wafer-level FBAR device variation on fabrication process. Regarding to the Mg-doping effect in MgxZn1-xO piezoelectric film, the amount of Mg in MgxZn1-xO film during the sputtering process must be properly controlled within 30% to keep the piezoelectric quality. The average acoustic speed of the Mg-doped ZnO film is 6870 m/s with the estimated range of 5760–7980 m/s, which is better than that of pure ZnO film (6330 m/s).

1. Introduction

Film bulk acoustic resonator (FBAR) is a promising RF device at the frequency ranging from 0.5 to 6.0 GHz due to its small size, high device power and strong potential application in both the cell phone market and sensor application [1–6]. Compared to surface acoustic devices (SAW) [7], FBAR is more powerful and advantageous especially for higher frequencies on 4G and 5G applications. Among the two types of FBAR devices, solid mounted resonator (SMR) is much more robust and therefore chosen in this work. FBAR built on silicon with Bragg reflector is also closer to CMOS integration [8] than SAW although it may also suffer from temperature sensitivity issues [9]. Just like a CMOS circuit that requires the MOSFET to have a controllable threshold voltage variation, FBAR device variation control is also essential to building an RF circuit such as duplexer in 4- and 5G mobile telecommunication systems. A duplexer demands that each FBAR in the circuit should have wafer-level homogeneity on the central frequency in RF performance as well as Q factor, and so on [10]. Although the FBAR product is commercially available in market, academic studies on the wafer-lever FBAR variation and process/design optimization are still relatively weak. In this paper, process variation effects on FBAR device performance were studied via various thin film depositions of Mg-doped $Mg_xZn_{1-x}O$ piezoelectric thin film by optimizing the sputtering power, pressure and ambient gas flow ratios as well as by altering sputtering targets (uniform $Mg_xZn_{1-x}O$ sputtering target with different Mg ingredient and dual sputtering targets of Mg and ZnO with independent control of sputtering power) and by post annealing treatment after the deposition. Design/process interactions and impacts on RF performance variation were studied via multi-FBAR device layouts in different sizes, locations and orientations on the same mask/wafer. Research work on FBAR wafer-level/wafer-to-wafer variation can be helpful to both the academic research study and industrial practice. RF characteristics

* Corresponding author.
E-mail address: franklinduan@sjtu.edu.cn (F.L. Duan).

https://doi.org/10.1016/j.sse.2018.10.015
Received 8 May 2018; Received in revised form 21 October 2018; Accepted 22 October 2018
Available online 24 October 2018
0038-1101/

were performed with RF probe station and network analyzer together with simulation tools to investigate the frequency shift with respect to process/design variation. The degree of C-axis orientation and crystalline properties of the $Mg_xZn_{1-x}O$ film were studied by XRD in the optimization process of piezoelectric layer.

The motivation of adding Mg in ZnO piezoelectric thin film lies in the enhanced resistivity due to the wider $Mg_xZn_{1-x}O$ bandgap and possible tailoring on FBAR resonant frequency [11]. Hu et al. [12] reported that incorporating Mg into ZnO may improve the Q factor in FBAR due to the enhanced longitudinal and horizontal acoustic speed and lower high frequency loss when Mg^{2+} replaced the Zn^{2+} in ZnO wurtzite structure. Park et al. [13] reported that the ingredient of Mg must be controlled since the ZnO's wurtzite structure would be shifted to hexagonal structure with over-dosed Mg ingredient, which would degrade the piezoelectric properties of this $Mg_xZn_{1-x}O$ thin film. Taking these effects in mind, different extents of Mg doped in ZnO thin films were attempted, in this paper, to compare their impacts on RF performance with the aid of varying the Mg ingredient in uniform $Mg_xZn_{1-x}O$ sputtering target and of dual target sputtering of Mg and ZnO under independent control.

2. Experimental

2.1. Mask design

Two layers of metals are needed to form FBAR devices as the top and bottom electrodes. Usually both layers need to be patterned based upon the need of device and RF circuits such as a duplexer. In this work, only the top metal is photolithography-patterned to build FBAR devices while the bottom metal is a uniform layer serving as an interconnect. This is sufficient for the purpose of studying the FBAR device wafer-level variation. Shown in Fig. 1, the center and ring metal electrodes form one pair of FBAR devices interconnected via the bottom uniform metal layer. The probing of this FBAR device follows standard GSG (ground-signal-ground) microwave probing patterns (70 μm width with 50 μm spacing). Different sizes of FBAR devices were designed on the same mask, to compare the wafer-level variation and possible size impacts on FBAR devices. The sizes of FBAR vary from 0.03 to 0.12 mm^2 (the area of the center square). The area ratio between the center square and the surround ring areas was kept as 1/10 for all devices.

2.2. FBAR fabrication process

To facilitate the future SOC integration, the substrate was chosen as

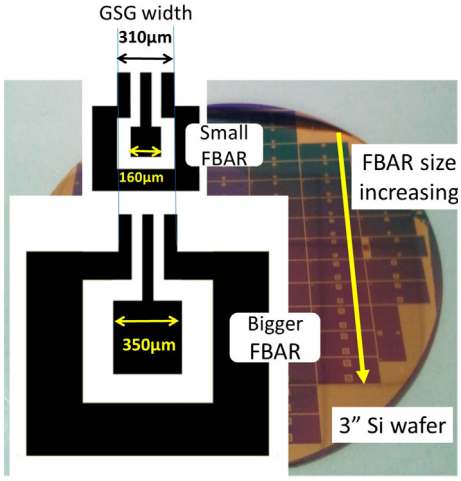

Fig. 1. Various size of FBARs ranging from 0.03 to 0.12 mm^2 (from top to bottom) were designed on the same mask fitting the 3″ silicon wafer with a total of ~100 FBAR devices.

Table 1
Sputtering parameters depositing the FBAR thin film layers.

Deposition parameters	$Mg_xZn_{1-x}O$	SiO2	W
Base pressure (Pa)	$< 5 \times 10^{-4}$	$< 5 \times 10^{-4}$	$< 5 \times 10^{-4}$
RF power (W)	100–250	180	100
Ar/O_2 flow rate (sccm)	40/0 –10/30	40/0	20/0
Sputtering pressure (Pa)	1.0–2.5	2.5	2.5
Substrate temperature (C)	300	300	300

3-inch (1 0 0) silicon wafer with thickness of 325 ± 25 μm and the resistivity of 20 Ω cm. Prior to piezoelectric film deposition, Bragg acoustic refection layer was built with three alternative layers of W and SiO_2 films with thickness of 500 nm and 600 nm, equivalent to the λ/4 resonance wavelength [13]. Their depositing parameters are summarized in Table 1.

The thickness of 90 nm Ti was deposited as bottom electrode on the Bragg reflector and then $Mg_xZn_{1-x}O$ thin film was deposited consequently at the same sputtering chamber to ensure a clean adherent surface. Also, shown in Table 1 is the range of process optimization parameters of piezoelectric film such as RF power, ambient pressure, and flow ratio to achieve the best piezoelectric $Mg_xZn_{1-x}O$ film. After piezoelectric film deposition, 150 nm-thick top electrodes were deposited and patterned. The 3D-view of FBAR was inspected by Keyence's VK-X 3D Laser Scanning Microscope, which was capable of performing noncontact profile and thickness measurements with a 0.5 nm z-axis resolution, as shown in Fig. 2.

Highly-ordered crystallographic film with a perfect (0 0 2) orientation is essential to building high quality FBARs, since piezoelectric response is highly dependent on the (0 0 2) orientation of this layer. In addition to the optimization of sputtering conditions listed in Table 1, the following design of experiments were also carried out:

- Using two kinds of $Mg_xZn_{1-x}O$ sputtering targets with Mg of 10% and 30% ingredient (in mole) respectively for $Mg_xZn_{1-x}O$ thin film sputtering;
- Varying the sputtering power of two independent Mg and ZnO sputtering targets to modify the Mg mole content in $Mg_xZn_{1-x}O$ film;
- The dependency of RF performance on FBAR size to improve the crystallization on (0 0 2) orientation in $Mg_xZn_{1-x}O$ film.

During the sputtering, a mixture of argon (Ar) (99.999%) and oxygen (O_2) (99.999%) was used as sputtering gas. The distance between the target and substrate is about 70 mm and target diameter is about 80 mm. The substrate temperature was kept 300 °C.

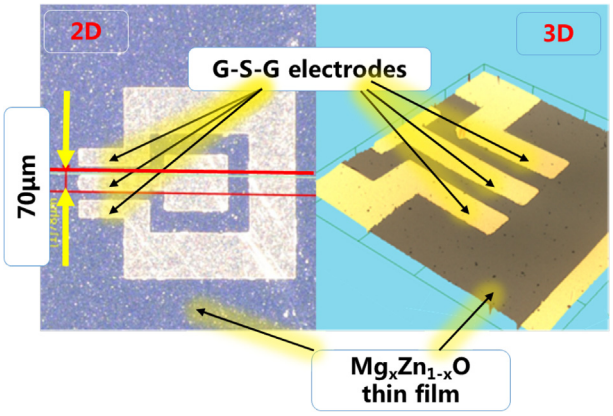

Fig. 2. top and 3D Microscope of FBAR device with standard 70-50-60-50-70 μm GSG Pico probe. Electrode material either Al or Au with thickness of 150 nm.

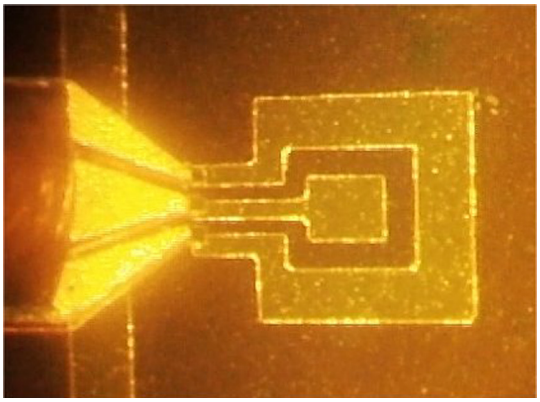

Fig. 3. RF prober and FBAR device with ACP 40 G-S-G Pico probe.

2.3. Characterizations

The crystalline characterization of piezoelectric thin film was performed by X-ray diffraction (XRD, D/max 2200/PC). The cross-sectional structure was observed by field emission scanning electron microscope (FESEM, Carl Zeiss Ultra55). The FBARs were probed on the wafer-level using Cascade 9000 TM probe station with an ACP 40 G-S-G Pico probe (Fig. 3) and the frequency resonance S-parameters of the FBARs were characterized using Keysight E5063A ENA Series Network Analyzer. The measured data and quality factors were extensively analyzed using Cascade WinCal XE 4.5.1 calibration and measurement system together with ADS (Advanced Design System) electronic design automation software system (Agilent ADS 2013).

2.4. Computer simulation on FBAR

Simulation was also conducted to help analyze the S11 characteristics of the FBAR. The simulation structure is shown in Fig. 4(a), incorporating a 3D FBAR structure. FBAR dimensions including piezoelectric film and electrode metal thickness follow our previous SEM measurements. The topmost layer of the resonator is an aluminum electrode patterned according to the FBAR size in the experiment (from 0.03 mm^2 to 0.12 mm^2). For the sake of easily carrying out the simulation without affecting the essence of the SMR FBAR device, the material of the sandwich Bragg reflector is replaced by the air as a perfect acoustic reflection layer below the FBAR active area. The simulation result is illustrated in Fig. 4(b), the piezoelectric film displacement at resonance (when the scanned frequency is at center resonant frequency). It is seen from our simulation that the peak vibrating amplitude of the piezoelectric layer can achieve the range of a few microns.

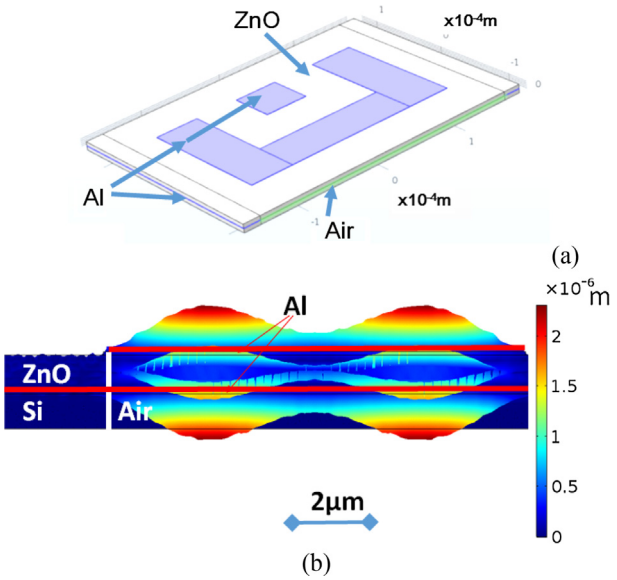

Fig. 4. The 3D simulation structure of FBAR device (a) and a demonstration of displacement of the piezoelectric film at resonant frequency (b).

Assuming a minor lattice modulation by adding Mg element in $Mg_xZn_{1-x}O$ film, piezoelectric material parameters of ZnO [14] were used in simulation as a rough estimate of Mg doped ZnO thin film material:

The Coupling matrix:

$$e = \begin{bmatrix} 0 & 0 & 0 & 0 & -0.048 & 0 \\ 0 & 0 & 0 & -0.048 & 0 & 0 \\ -0.567 & -0.567 & 1.320 & 0 & 0 & 0 \end{bmatrix} \ C/m^2$$

Elasticity matrix:

$$c = \begin{bmatrix} 2.09714 & 0 & 0 & 0 & 0 & 0 \\ 1.2014 & 2.09714 & 0 & 0 & 0 & 0 \\ 1.05359 & 1.05359 & 2.1194 & 0 & 0 & 0 \\ 0 & 0 & 0 & 0.423729 & 0 & 0 \\ 0 & 0 & 0 & 0 & 0.423729 & 0 \\ 0 & 0 & 0 & 0 & 0 & 0.442478 \end{bmatrix} \times 10^{11} \ Pa$$

and the relative permittivity matrix:

$$\varepsilon = \begin{bmatrix} 8.5446 & 0 & 0 \\ 0 & 8.5446 & 0 \\ 0 & 0 & 10.204 \end{bmatrix}$$

The simulation model incorporates mechanical and electrical losses in the piezoelectric ZnO film, representing the hysteresis in a stress-strain curve and in the polarization versus electric field curve of the piezo-material. Both structural and electrical equations were solved in considerations of the multi-physics piezoelectric effect. The electrical equations are not solved in the metallic aluminum layers because the aluminum has a much higher conductivity than that of zinc oxide and hence the aluminum layers almost act as equipotential regions. The dominant electromechanical coupling is exhibited by the piezoelectric layer only. The admittance is calculated as the ratio of the total current flowing through the piezoelectric material to the voltage across it. It is a complex-valued quantity and the imaginary part reflects the displacement current while the real part reflects the conduction current as well as other losses in the structure. The structural and dielectric loss factors appear as the imaginary components of the mechanical stiffness and relative permittivity respectively. The admittance is then calculated and plot as a function of frequency, in comparison with our experimental data on RF measurements.

3. Results and discussion

3.1. Process optimization of $Mg_xZn_{1-x}O$ film

(1) Optimization of sputtering conditions

First, various sputtering conditions such as RF power, sputtering pressures, Ar/O_2 ratio were optimized to achieve best C-axis piezoelectric orientation of the $Mg_xZn_{1-x}O$ thin film. The target is to achieve a stronger and sharper diffraction peak in XRD as well as its minimum deviation from the (0 0 2) 2θ value (34.422° for ZnO). After a series of experiments, the optimized condition on depositing $Mg_xZn_{1-x}O$ thin film is chosen as 200 W sputtering power, 2.5 Pa of depositing pressure, and 300 °C of substrate temperature with Ar/O_2 ratio of 40:0. The diffraction peak of the obtained $Mg_xZn_{1-x}O$ (0 0 2) is strong and sharp with FWHM value of 0.4°, and the value of residual stress of multilayer films is 2.07 GPa. One of the XRD chart for the optimization of RF power is shown in Fig. 5 where the optimized sputter power is chosen as 200 W instead of 250 W, even if the peak is higher due to its wider

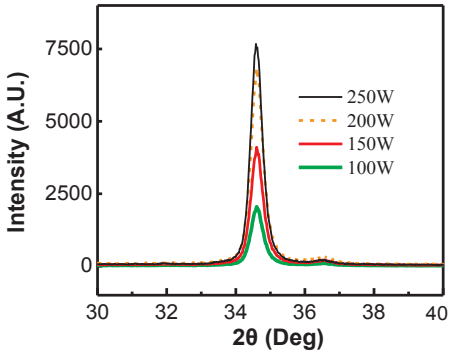

Fig. 5. The XRD patterns of the $Mg_xZn_{1-x}O$ films with different RF powers. Ar/O_2 ratio is 40:0, substrate temperature 300 °C, and pressure 2.0 Pa.

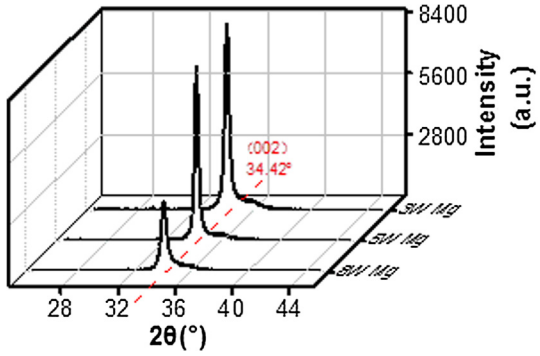

Fig. 6. XRD of various Mg-doped ZnO using different sputtering power on Mg target while keeping the sputtering power of ZnO target as 400 W.

FWHM (Full Width at Half Maximum).

(2) Optimization on Mg content in the $Mg_xZn_{1-x}O$ film

Two $Mg_xZn_{1-x}O$ sputtering targets with Mg content of 10% and 30% were used to form the $Mg_xZn_{1-x}O$ layer under the same sputtering process condition. Table 2 lists the corresponding diffraction peak and 2θ value of (0 0 2) orientation, as well as derived FWHM and grain size. The diffraction peak in both cases are very high while the peak position (2θ) in the case of 30% Mg has more deviation from (0 0 2), agreeing with the result in Zhang's [15] work that over-dose of Mg in $Mg_xZn_{1-x}O$ degrades the wurtzite structure property in ZnO by shifted peak position from (0 0 2) 2θ angle of ZnO 34.4°.

Similar approach to achieve different Mg-doping in $Mg_xZn_{1-x}O$ is via the dual sputtering targets of Mg and ZnO in the same chamber by a fixed RF power of ZnO sputtering target at 400 W while altering the sputtering power on Mg target as 3, 5 and 8 W. Increasing the sputtering power of Mg target adds more Mg ingredient in $Mg_xZn_{1-x}O$ film. The XRD result is shown in Fig. 6. The corresponding diffraction peak amplitude, position and FWHM value are compared in Table 3. It is observed that in this approach, overdose of Mg ingredient degrades diffraction amplitude and causes more deviated (0 0 2) orientation, consistent with the previous conclusion that doping ingredient of Mg in $Mg_xZn_{1-x}O$ film must be carefully controlled [15] in the optimization process.

Comparing the two methods of Mg-doping, an overall sharper XRD peak is observed (by comparing Table 2 and 3) by the first method (using a uniform $Mg_xZn_{1-x}O$ target) than the second (using separate Mg and ZnO sputtering targets) with fairly similar (0 0 2) orientation qualities, and therefore a uniform 10% Mg-doped $Mg_xZn_{1-x}O$ sputtering target is chosen to fabricate the piezoelectric thin film in our FBAR device.

(3) Effect of post-sputtering annealing

Samples with the optimized sputtering conditions above were annealed under various temperatures in N_2 ambient for 10 min. The XRD results are shown in Fig. 7. It is seen that diffraction peak becomes higher and narrower after annealing yet with more 2θ deviation. It is therefore not as conclusive that the annealing has positive impacts for a better (0 0 2) crystallization on ZnO film formation in the process of

Table 2
XRD results of different Mg contents.

Sputter target of $Mg_xZn_{1-x}O$	2θ (°)	Δ2θ (from 34.22°)	Height (A.U.)	FWHM (°)	Grain size (nm)
30%Mg	35.502	1.081	22,496	0.208	58.6
10%Mg	34.113	−0.308	261,692	0.325	26.8

Table 3
XRD results of various Mg sputtering power.

Sputter power	2θ (°)	Δ2θ (from 34.22°)	Height (A.U.)	FWHM (°)	Grain size (nm)
3 W Mg	34.176	−0.245	8322	0.395	21.7
5 W Mg	34.256	−0.165	7829	0.342	27.3
8 W Mg	34.114	−0.307	3061	0.504	17.4

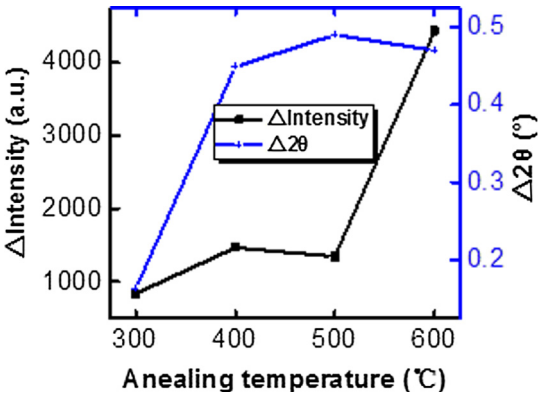

Fig. 7. Effect of annealing on XRD result of MgxZn1-xO piezoelectric film: refraction intensity and the deviation of 2θ from (0 0 2) orientation.

SMR FBAR fabrication. Currently, our FBAR fabrication is based on the samples without annealing, and further research work is ongoing to study the overall annealing impacts on the piezo-electric quality by measuring the RF characteristics of FBAR devices built on these annealed wafers.

(4) SEM on cross sectional morphology of FBAR

With optimized piezoelectric film deposition, various FBAR devices were fabricated and Fig. 8 is a cross-sectional view of $Mg_xZn_{1-x}O$/Ti/Bragg layered structure of SMR FBAR. All layers are clearly visible and the interfaces between $Mg_xZn_{1-x}O$ film/Ti/Bragg reflector layers are distinct. Thickness of SiO_2 and W layer as well as the bottom electrode Ti layer are close to our target thickness (~500–600 nm and 90 nm). The thickness of Mg-doped ZnO film is ~1.7 μm according to the SEM measurements, close enough to their expected value. The thickness variation is in the range of 1.6–1.9 μm (not seen in this picture) from site to site on the wafer.

3.2. FBAR device variation studies

Various FBARs are characterized to compare the size effect on FBAR devices and the wafer-level and wafer-to-wafer variations on Smith

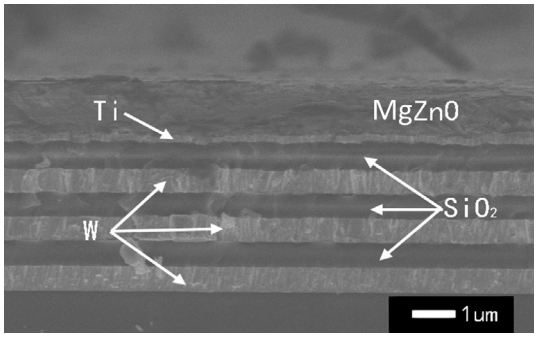

Fig. 8. Cross-sectional view of FBAR structure with Bragg reflection layer.

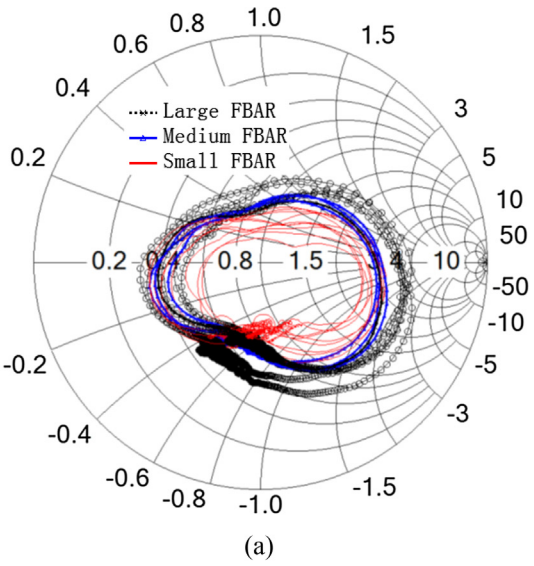

Fig. 9. Characteristics of $Mg_xZn_{1-x}O$ based FBARs on one wafer with different FBAR sizes. (a) Smith chart, (b) S_{11} Return loss. Thin red lines, the blue triangle and the big black symbols are the FBAR samples with area of 0.03 mm^2, 0.06 mm^2 and 0.12 mm^2 respectively. (For interpretation of the references to colour in this figure legend, the reader is referred to the web version of this article.)

chart, impedance and phase response by one-port measurement of the reflection coefficient S11. The RF probes and the network analyzer were properly calibrated prior to the measurement. Fig. 9 shows the RF

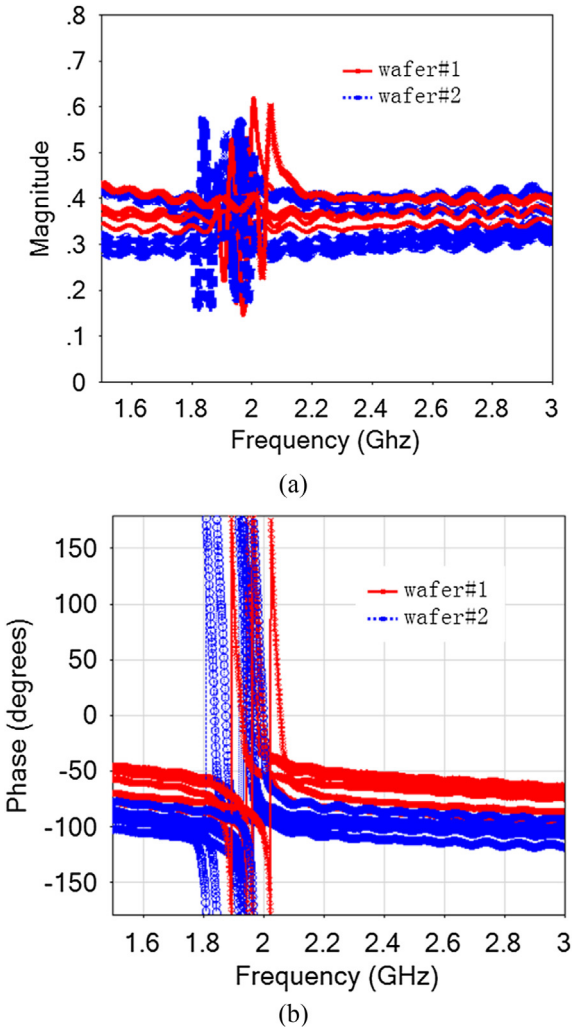

Fig. 10. Wafer-level and wafer-to-wafer FBAR device variations s in two different wafers. (a) Impedance and (b) Phase. Red solid lines are FBARs from wafer#1; blue dashed square are from FBARs in wafer#2. (For interpretation of the references to colour in this figure legend, the reader is referred to the web version of this article.)

characteristics of different areas of FBARs. There are three sizes of FBARs being evaluated, with area of 0.03, 0.06 and 0.12 mm^2. Larger FBAR in general may have larger resonance circles in Smith chart and less frequency variation with overall less S11 return loss. This suggests a relatively larger FBAR area may average out the roughness turbulence of the deposited piezoelectric film. Obviously more delicate sputtering process help to reduce this variation and to achieve a good FBAR in smaller areas.

Fig. 10 shows RF measurements on FBAR devices on different locations on the two wafers (the repetition of the RF result (not shown) on the same FBAR is identical). It is seen that with the same process control the central frequency has a roughly 0.1 GHz shift between these two wafers. Within each wafer most FBARs confine their resonance frequencies within 0.2 GHz range with good resonance characteristics. Later simulation indicates that this central frequency variation is mainly due to the thickness variation of MgZnO piezoelectric film. More delicate process control is necessary to confine the central frequency in a tighter range in order to fabricate FBAR-related circuitry such as duplexer on various WIFI and sensor applications. This process variation of the FBARs is fairly homogenous with our consistent fabrication process, and it is also observed that yield level of FBAR devices on one wafer is fairly good (> 90%) just a few FBAR device are good once yet

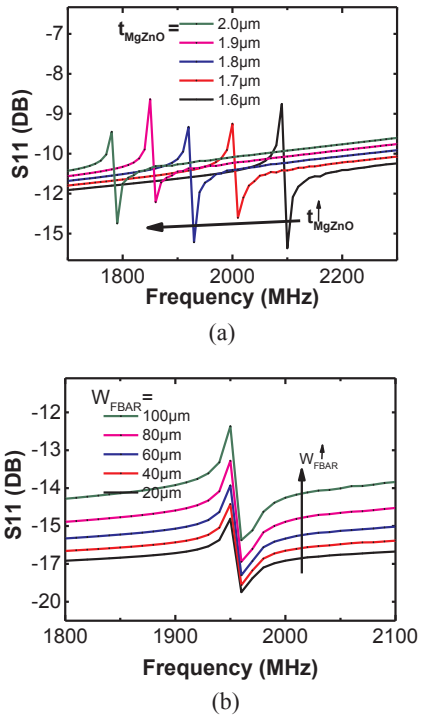

Fig. 11. Simulated FBAR frequency response variation due to the thickness variation (a) and the size (b) of FBAR. t_{MgZnO} is the piezoelectric film thickness and W_{FBAR} is the width of the FBAR device.

the chance of a successful wafer is fairly low (2 out of 10). The overall yield of FBARs and related RF circuitry may be acceptable in the fabrication cost aspect yet more delicate process control efforts are still needed for FBAR yield enhancement in general industry practice. Variation of FBAR performance with various orientations on the wafer are not obvious compared to the general wafer-level FBAR variations.

In general, a distinct resonant phenomenon with good return loss, between −10 and −20 dB, is achieved. The corresponding coupling coefficient keff^2 and quality factor Q values are calculated based upon the formula below [16]:

$$k_{eff}^2 = \frac{\pi^2}{4}\left(1 - \frac{fs}{fp}\right) \quad (1)$$

$$Q = \left|\frac{fp}{FWHM}\right|_{fp} \quad (2)$$

In the formula, f_s and f_p are the series and parallel resonance frequency and the FWHM is the full width at half maximum of parallel resonance frequency f_P. The calculated Q and keff^2 are in the range of 400–800 and 1.5–3% respectively.

The average calculated acoustic phase velocity is evaluated as in [16]:

$$f = \frac{v}{2d} \quad (3)$$

$$v = f \times 2d \quad \in \quad (f_{min} \times 2d_{min}, f_{max} \times 2d_{max}) \quad (4)$$

where v, f and d are the acoustic speed, central frequency and the thickness of Mg-doped ZnO piezoelectric thin film. The f_{min}/f_{max} and d_{min}/d_{max} are the minimum and maximum values of central frequency in our RF and film thickness measurements above. The central frequency range from 1.8 to 2.1 GHz and film thickness is in the range of 1.6–1.9 μm measured in SEM on MgZnO layer, and the corresponding resonance frequency of FBAR devices is 6870 m/s in average in the range of 5760–7980 m/s. Though this value is slightly better than the intrinsic acoustic speed of pure ZnO film (6330 m/s) [14], it is not yet conclusive of the enhanced acoustic speed due to the added Mg ingredient MgZnO piezoelectric film. Proper process variation control is necessary to correctly evaluate the acoustic speed value.

3.3. Simulation analysis

The impacts of the piezoelectric film thickness and the FBAR size on S11 response are analyzed via computer simulation. Fig. 11 shows the simulated S11 response by varying piezoelectric thin film thickness and FBAR device size. It is seen from the simulation (Fig. 11(a)) the frequency variation between 1.8 and 2.1 GHz correlate to the thickness variation of 1.6–2.1 μm, in consistent to the experimental data in Figs. 9 and 10, indicating that the frequency shift on the peak resonance in S11 is mainly attributed to the thickness variation and a thicker piezoelectric film induces a lower resonant frequency. The size of the FBAR devices The dependency of RF performance on FBAR affect the amplitude of the resonance peaks shown in Fig. 11(b); this is fairly consistent with the data shown in Fig. 9(b), where we observed a lower amplitude for smaller FBAR devices.

4. Conclusions

The thickness variation of the piezoelectric film plays a key role in controlling the central resonant frequency range in FBAR devices, which in the end affects the yield of the successful FBAR duplexer circuitry. Our optimized FBAR process control renders a 1.6–1.9 film wafer-level thickness variation and this causes 1.8–2.1 GHz wafer-level resonance frequency variation as well as wafer-to-wafer variation. Impact of film thickness on resonant frequency variation is verified by multi-physics computer simulation. The sizes of the FBAR devices only affect the amplitude of the resonance peaks. Regarding to the Mg-doping effect in $Mg_xZn_{1-x}O$ piezoelectric film, the amount of Mg in $Mg_xZn_{1-x}O$ film during the sputtering process must be properly controlled within 30% to keep the piezoelectric quality. The average acoustic speed of the Mg-doped ZnO film is 6870 m/s with the estimated range of 5760–7980 m/s. Although the average speed is slightly better than that of pure ZnO film (6330 m/s), the enhancement is not as conclusive due to the estimated speed variations caused by process variation of the piezoelectric film.

Acknowledgement

This work was supported by Chinese National Science Foundation (No. F040801). Special thanks to Dr. Xuecheng Fu in Center for Advanced Electronic Materials and Devices (AEMD), Liyun Shi in Instrumental Analysis Center and Junchen Liu in SEIEE of Shanghai Jiaotong University.

References

[1] Lakin KM, Wang JS. Acoustic bulk wave composite resonators. Appl Phys Lett 1981;38(3):125–7.
[2] Lakin KM. Thin film resonator technology. IEEE Trans Ultrason Ferroelect Freq Contr 2005;52:707–16.
[3] Ruby RC, Bradley P, Oshmyansky Y. Thin-film bulk-wave acoustic resonator (FBAR) for wireless applications. Proceedings of the IEEE ultrasonics symposium, vol. 1. 2001. p. 813–21.
[4] Liu Y, Shen Y, Duan LF. Solidly mounted resonators fabricated for GHz frequency applications based on MgxZn1-xO piezoelectric film. Vacuum 2017;141:254–8.
[5] Fattinger GG, Kaitila J, Aigner R, Nessler W. Thin film bulk acoustic wave devices for applications at 5.2 GHz. Proc IEEE ultrason symp. 2003. p. 174–7.
[6] Campanella H. Thin-film bulk acoustic wave resonators (FBAR): fabrication, heterogeneous integration with CMOS technologies and sensor applications. Doctoral dissertation; 2007.
[7] Newell WE. Face mounted piezoelectric resonators. Proc IEEE 1965;53(6):575–81.
[8] Satoh Y, Nishihara T, Yokoyama T, Ueda M, Miyashita T. Development of piezoelectric thin film resonator and its impact on future wireless communication systems. Jpn J Appl Phys 2005;44.5A:2883.
[9] Wang K, et al. Design of A 1.8-mW PLL-free 2.4-GHz receiver utilizing temperature-compensated FBAR resonator. IEEE JSSC 2018;53(6).

[10] Paco PD, Corrales E, Verdu J, Menendez O. A review of recent patents on bulk acoustic wave resonators and filters. Rece Pat Electr Electr Eng 2009;2(2).
[11] Liu L, Mei Z, Tang A, Liang H, Du X. Self-compensation induced high-resistivity in MgZnO. J Phys D Appl Phys 2017;50(6):065102.
[12] Hu Y, Cai B, Hu Z, Liu Y, Zhang S, Zeng H. The impact of mg content on the structural, electrical and optical properties of mgzno alloys: a first principles study. Curr Appl Phys 2015;15(3):423–8.
[13] Park SH, Ahn D. Spontaneous and piezoelectric polarization effects in wurtzite ZnO/MgxZn1-xO quantum well lasers. Appl Phys Lett 2005;87(25):3509.
[14] Morkoc H, Ozgur U. Zinc oxide: fundamentals, materials and device technology. Berlin: Wiley-VCH; 2009.
[15] Zhang X. Preparation and characterization of MgxZn1-xO films Doctoral dissertation China: Shandong University; 2006.
[16] Zhang Y, Chen D. Multilayer integrated film bulk acoustic resonators. Berlin: Springer; 2012.

Franklin Li Duan got his M.E. and B.E. in Tsinghua University in China in 1987 and 1985 respectively, in a major of Microelectronics. In 1998 he got his Ph.D. in George Mason University in Virginia, in the School of Information and Engineering Technology. He has over 15 years' experience in Silicon Valley in IC industry. He joined Shanghai Jiaotong University, School of Electronics Information and Electrical Engineering, focusing on RF devices for wireless-related application.